energies

MDPI

Article

Plasma-Deposited Fluorocarbon Coatings on Methylammonium Lead Iodide Perovskite Films

Vincenza Armenise [1], Silvia Colella [2,*], Antonella Milella [1,*], Fabio Palumbo [2], Francesco Fracassi [1,2] and Andrea Listorti [1]

[1] Department of Chemistry, University of Bari Aldo Moro, Via Orabona 4, 70125 Bari, Italy; vincenza.armenise@uniba.it (V.A.); francesco.fracassi@uniba.it (F.F.); andrea.listorti@uniba.it (A.L.)
[2] National Research Council, Institute of Nanotechnology (CNR-NANOTEC), c/o Department of Chemistry, 70125 Bari, Italy; fabio.palumbo@cnr.it
* Correspondence: silvia.colella@nanotec.cnr.it (S.C.); antonella.milella@uniba.it (A.M.); Tel.: +39-080-544-2009 (S.C.); +39-080-544-2858 (A.M.)

Abstract: Metal halide perovskites are excellent semiconductors materials that can be exploited in many fields, from the vastly explored photovoltaics to the recent applications in photocatalysis. One of the material's known limitations is the poor resistance to moisture which induces degradation, triggered by the soft and defective nature of its surface. In this study, we explore non-equilibrium plasmas, to deposit a fluorocarbon polymer on the surface of a $MAPbI_3$ film. We found that the treatment generally enhances the film stability over time, and in certain conditions it improves the perovskite optical properties, demonstrating to be a good strategy aiming defects passivation. Thanks to the solvent-free and non-invasive nature of plasmas, this technique has the potential to be extensively applied to a wide range of perovskite materials targeting different applications.

Keywords: plasma deposition; fluorocarbon coating; metal halide perovskite; methylammonium lead iodide film; perovskite stability

check for updates

Citation: Armenise, V.; Colella, S.; Milella, A.; Palumbo, F.; Fracassi, F.; Listorti, A. Plasma-Deposited Fluorocarbon Coatings on Methylammonium Lead Iodide Perovskite Films. *Energies* **2022**, *15*, 4512. https://doi.org/10.3390/en15134512

Academic Editor: Adalgisa Sinicropi

Received: 19 May 2022
Accepted: 18 June 2022
Published: 21 June 2022

Publisher's Note: MDPI stays neutral with regard to jurisdictional claims in published maps and institutional affiliations.

Copyright: © 2022 by the authors. Licensee MDPI, Basel, Switzerland. This article is an open access article distributed under the terms and conditions of the Creative Commons Attribution (CC BY) license (https://creativecommons.org/licenses/by/4.0/).

1. Introduction

Plasmas are traditionally distinguished in equilibrium (i.e., thermal) and non-equilibrium (i.e., non-thermal) ones. The working pressure is usually considered the discriminating factor between these two categories [1,2]. An equilibrium plasma (e.g., arc discharge or plasma torch) typically develops if the gas pressure is higher than 10 Torr and is characterized by a similar electron as gas temperatures. The non-equilibrium conditions are frequently generated at low pressure (LP) since most of the energy delivered to the plasma remains channelled as electron kinetic energy, while the translational gas temperature remains close to room temperature [1]. However, these conditions can be obtained also operating at atmospheric pressure (AP) using specific experimental strategies [3,4]. Non-equilibrium plasma processes have attracted increasing attention thanks to their unique capability to modify the material's surface, without affecting the bulk properties [1,5]. Herein (i) the plasma deposition of organic, inorganic, or hybrid multicomponent thin films, (ii) the plasma treatment of materials surfaces through grafting of chemical groups and/or cross-linking mechanisms, and (iii) the plasma etching consisting of the ablation of material from the substrate surface can be discerned [1,5,6]. Plasma processed materials can be considered an entirely novel class of materials with tuneable properties, very interesting in several technological fields that demand, for example, biocompatible materials [7,8], dyeable textiles [9], adsorbent materials for heavy metal removal [10,11], thin films for water splitting [12], superhydrophilic or superhydrophobic foams for oil/water separation [13].

Over the last few years, the use of the plasmas for the modification of metal halide perovskite (MHPs) films has increasingly gotten the attention of the community. MHPs are hybrid semiconductors material that are revolutionizing photovoltaic technologies and can

also be suitable for solar-driven photocatalysis [14–18]. They are characterized by superior properties such as high optical absorption in the visible region, easy tuneable band-gap, large ambi-polar carrier diffusion, and straightforward deposition processing [19–25]. During the practical applications of the MHPs films, external parameters (e.g., illumination, thermal stress, moisture, exposure to solvents) can affect the perovskite stability causing the collapse or the transformation of their crystalline network [18,26–29]. However, what hinders their applications as photocatalysts and their commercialization as solar converting devices or more in general optoelectronic devices is the known instability to moisture. Strategies aimed at solving this issue would represent a breakthrough in the field [18,23,24,30]. In particular, one of the most critical issues for the MHP thin film stability seems to lay on their surface, where the highest concentration of defects and uncoordinated ions are. The resulting soft nature of the perovskite interface makes it susceptible to attack from ambient species and water. For example, the presence of organic terminations on the surface of the referential $MAPbI_3$ has been demonstrated to trigger the infiltration of water within the film, causing a very rapid decomposition of the material to a hydrated perovskite phase as to PbI_2 [18,27,31,32]. Therefore, the possibility to use plasma to tune their surface allowing them to further improve their performances and/or their stability would represent an interesting frontier for scientific research. Some studies on the application of plasma treatment and/or etching on perovskite films have been reported in the literature [33–41]. Particularly, Kim et al. [33] treated methylammonium lead iodide ($MAPbI_3$) perovskite layers with an H_2-containing AP plasma for patterning their surface. Xiao et al. [34] and Li et al. [35] employed Ar fed plasmas to modify the surface composition of the $MAPbI_3$ film. The effects of ambient-air plasma treatment and of an LP O_2 one on perovskite films were examined [36–38], and some studies analysed the effects of plasma treatments on the $MAPbI_3$ coatings directly performed in the nitrogen-filled glove box, necessary for the perovskite deposition [39–41].

In this work we report for the first time, to the best of our knowledge, the plasma enhanced chemical vapour deposition (PECVD) of fluorocarbon coatings directly performed on $MAPbI_3$ perovskite films, with the specific aims of enhancing the MHP hydrophobicity and simultaneously modifying its surface. Fluorocarbon polymers are indeed characterized by unique properties (e.g., water repellence, high thermal stability, chemical resistance, low friction coefficient, low refractive index) attracting significant attention for technological use, such as antifouling films, biocompatible surfaces, liquid resistant paper and materials for microelectronics with low dielectric constant [42,43], but also for the purpose of our work [44]. However, the application of fluorocarbon coatings on desired substrates is difficult to obtain due to their inert nature. Conventional deposition methods involve the utilization of catalysts, surfactants, crosslinking agents, etc., and suffer from processing issues, such as low control of the coatings thickness and poor adhesion to the materials [42]. The PECVD is an effective and extensively studied solvent-free single-step process to realize fluorocarbon thin films, allowing their polymerization with good adhesion on a wide range of substrates as control over thickness, chemical composition, and final properties, such as hydrophobicity and water repellence [1,42,43,45–47]. Among the other deposition methods, it can be considered very useful because it allows depositing adhered fluorocarbon coatings onto organic or inorganic substrates of different shapes, and geometry as surface chemistry transfers minimal thermal stress and degradation to them [42].

As a preliminary investigation, we report the results of the fluorocarbon coatings polymerized on silicon substrates using the PECVD. Fourier-transform infrared (FT-IR) as X-ray photoelectron spectroscopy (XPS) analyses were carried out to examine the chemical composition, while thickness and static water contact angle (WCA) measurements were performed to determine the coating deposition rate and the wettability. Fluorocarbon layers were then deposited on the $MAPbI_3$ films and their effect on the perovskite properties was verified by scanning electron microscopy (SEM) images, ultraviolet–visible (UV-vis) absorption spectra, photoluminescence (PL) measurements. Finally, stability tests were performed to assess the efficacy of the hydrophobic coating as protection towards humidity.

2. Materials and Methods

2.1. Substrates Treatment

Glass substrates (15 mm × 15 mm, 1 mm thick) were treated using a home-made AP plasma reactor with a symmetrical parallel-plate dielectric barrier discharge (DBD) electrode configuration [10,48]. Each electrode (50 × 50 mm^2) consisted of an Ag-Pd metallization layer deposited on an Al_2O_3 plate with a thickness of 0.635 mm. The electrode assembly was located in a Plexiglas chamber, kept at a constant pressure of 760 Torr through a diaphragm pump. Before each plasma process, the chamber was purged with 6 slm of He for 5 min to remove air contaminations, then a feed mixture of He and O_2 (Air Liquide, Paris, France, 99.99% purity) was homogenized for 5 min [10,37]. Specifically, as controlled by mass flow controllers (MFC), the He flow rate was kept fixed at 6 slm while the O_2 concentration in the mixture was equal to 0.5%. To ignite the discharge, a 20 kHz sinusoidal alternated current (AC) high voltage (HV) of 1.05 kV_{rms} was applied to the electrodes (4 mm gas gap) [10]. The plasma treatment was performed for 60 s.

2.2. Perovskite Films Deposition

The perovskite films were deposited in a nitrogen-filled glove box (Jacomex, Dagneux, France). A 48 wt% solution of N,N-dimethylformamide anhydrous (DMF, 99.8%, Sigma-Aldrich, St. Louis, MO, USA), containing 1:1:1 mol of Methylammonium iodide (MAI, Greatcellsolar, Queanbeyan, Australia), PbI_2 (Alfa Aesar) and anhydrous dimethyl sulfoxide (DMSO, 99.9%, Sigma-Aldrich) was prepared. The solution was spin-coated onto the treated substrates by a spin-coating process at 4000 rpm for 25 s with a dripping of anhydrous toluene (99.8%, Sigma-Aldrich) at 15 s before the end of the spinning. The obtained films were subsequently annealed onto a hot plate (100 °C, for 10 min) and then cooled to room temperature.

2.3. Plasma Deposition of Fluorocarbon Coatings

Fluorocarbon coatings were deposited in a cylindrical parallel plate stainless steel plasma reactor evacuated by a turbomolecular/rotary system [49]. The upper shower electrode was characterized by a diameter of 15 cm and it was connected to a radiofrequency (RF, 13.56 MHz) power supply (Cesar 1310, Dressler) through an impedance automatic matching unit (ULVAC, model 002A). During the deposition processes, the power delivered to the electrode was fixed to 20 W. The lower electrode (19 cm in diameter) was connected to the ground (GND), it was set 5 cm apart from the upper RF electrode and acted as a sample holder. The pressure in the chamber was fixed at 100 mTorr and monitored by means of a capacitive Baratron (MKS Instruments, Andover, MA, USA). The Hexafluoropropene (C_3F_6, Sigma Aldrich, ≥99%) vapors flow rate was set to 6 sccm with an electronic mass flow controller (MKS Instruments). The deposition time was varied in the range of 10–120 s. Specifically, it was set to 10 s, 30 s, 60 s, or 120 s.

2.4. Samples Characterization

FT-IR analyses of the fluorocarbon coating deposited on silicon double-polished substrates were carried out with a FT-IR Bruker Vertex 70 V spectrometer. Spectra were collected, under vacuum, in the range of 400–4000 cm^{-1} over 32 scans with a resolution of 4 cm^{-1}, and their baseline was subsequently corrected.

XPS analyses were performed with a Scanning XPS Microprobe (PHI 5000 Versa Probe II, Physical Electronics) equipped with a monochromatic Al Kα X-ray source (1486.6 eV), operated at 15 kV and 24.8 W, with a spot of 100 μm. Survey (0–1200 eV) and high-resolution spectra (C1s, F1s) were recorded in FAT (Fixed Analyser Transmission) mode at a pass energy of 117.40 and 29.35 eV, respectively. The analyser energy resolution, evaluated on the FWHM Ag 3d5/2 photoemission line, was 0.7 eV for a pass energy of 29.35 eV. A dual beam charge neutralization, with a flux of low energy electrons (~1 eV) combined with very low energy positive Ar^+ ions (10 eV), was used to compensate for surface charging. The hydrocarbon component of the C1s spectrum, fixed at 284.8 eV, was used as the internal

standard for charging correction. All spectra were collected at an angle of 45° with respect to the sample surface. Best-fitting of the C1s and F1s spectra was carried out with MultiPak data processing software.

Coatings thickness was determined with a D-120 KLA Tencor stylus profiler on partially masked samples averaging results over 5 different measurements on each sample. The deposition rate of plasma-deposited coatings was calculated by dividing the film thickness by the deposition time and it was equal to 0.7 $nm \cdot s^{-1}$.

Static WCA measurements of plasma-deposited coatings were performed with a KSV CAM 200 instrument, using 2 μL water droplets. The WCA values were obtained by averaging results for three different samples (three measurements per one).

A Zeiss SUPRA 40 field emission scanning electron microscope (FESEM) was applied to investigate the morphology of perovskite films with and without the fluorocarbon coatings. Before SEM observations each sample was sputter-coated with 30 nm of Cr using a turbo-pumped sputter coater (Quorum Technologies, Lewes, UK, model Q150T). Images were acquired with the in-lens equipped detector at a working distance in the range of 2.2–3.6 mm, electron acceleration voltage (extra-high tension) of 3.00 kV, and magnification in the range of 10–100 kX.

Atomic Force Microscopy (AFM) images were acquired using a XE-70 microscope (Park Systems, Suwon-si, Korea) in non-contact mode using PPP-NCHR probes from Nanosensors with a resonance frequency of 330 kHz.

The UV-vis absorption spectra were recorded with an Agilent Cary 5000 UV-vis-NIR spectrophotometer in the 200–800 nm wavelength range at room temperature.

The PL measurements were recorded by means of a Fluorolog®-3 spectrofluorometer (HORIBA Jobin-Yvon, Edison, NJ, USA), equipped with a 450 W xenon lamp as the exciting source and double grating excitation and emission monochromators. All the optical measurements were performed at room temperature on powder dispersed samples as obtained from the synthesis without any size sorting treatment. The PL emission spectra were recorded by using an excitation wavelength of 375 nm [50].

2.5. Stability Tests

Pristine $MAPbI_3$ films and reference samples realized by the plasma deposition, of the fluorocarbon coating carried out on the perovskite layer for 10 and 60 s were exposed to open air (humidity in the range of 35–48%, the temperature of 25 °C) for 8 weeks to evaluate their stability. Photographs of these samples were acquired as a function of the exposure time. UV-vis absorption spectra were recorded using an Agilent Cary 5000 spectrophotometer as previously described. The same samples were also stored in a glass chamber at a humidity of 50% and temperature of 25 °C for 48 h. Photographs were captured to monitor their stability.

3. Results and Discussion

The FT-IR spectrum of the plasma-deposited coating is reported in Figure 1. It shows absorptions in the range 406–1850 cm^{-1}, typical of plasma polymerized fluorocarbon polymers, confirming the successful deposition of this typology of coating [1,42,45,49].

The main spectral feature is the broad band between 1050 and 1400 cm^{-1} due to CF_x stretching vibrations: the shoulder at about 1340 cm^{-1} is due to CF groups while the one at 1160 cm^{-1} is assigned to the symmetric stretching of CF_2. Furthermore, the CF_3 band at 981 cm^{-1} and the amorphous band at 740 cm^{-1} are present. Finally, the band peaked at 1730 cm^{-1} due to absorptions from C=C (e.g., $C{=}CF_2$, $CF{=}CF_2$) and C=O. The C=O bonds are formed in the plasma deposited films due to the oxidation of dangling bonds after atmosphere exposure.

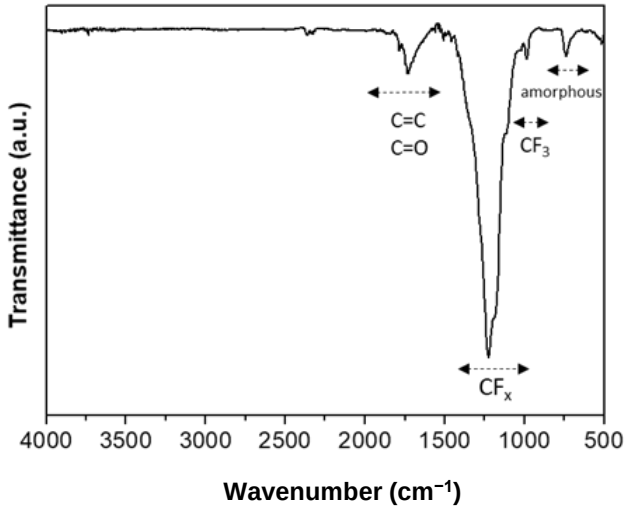


Figure 1. FT-IR spectrum of the fluorocarbon coating plasma-deposited on a silicon substrate.

In Table 1, the XPS surface atomic concentrations of the plasma-deposited coating are reported. Reported data confirm the presence of oxygen in traces, as a contaminant. Furthermore, the F/C and O/C atomic ratios correspond to 1.36 and 0.02, respectively.

Table 1. XPS surface atomic concentrations of the plasma-polymerized coating deposited on a silicon substrate.

Sample	C (at %)	F (at %)	O (at %)	F/C	O/C
Plasma-deposited coating	42.1	57.2	0.7	1.36	0.02

In order to gain deeper information on the surface chemical structure of the coating, the high-resolution C1s spectrum was curved-fitted and the results are shown in Figure 2. The spectrum is broad, as typically obtained by plasma polymerization, and reveals the presence of several functional groups: C-C/C-H (284.8 ± 0.2 eV), C-CF/C-CF_2 (286.4 ± 0.2 eV), C=CF (287.8 ± 0.2 eV), CF (289.0 ± 0.2 eV), CF_2 (291.0 ± 0.2 eV) and CF_3 (293.1 ± 0.2 eV) [49,51]. The presence of several fluorinated groups is due to the fragmentation of the C_3F_6 molecule in the plasma and to the ion bombardment of the film during growth. The F1s spectrum is peaked at 688.2 eV (spectrum not reported), in agreement with its covalent nature.

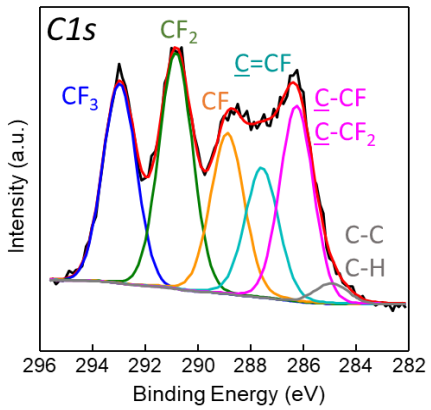


Figure 2. XPS C1s high-resolution spectrum of the plasma-polymerized coating.

The wettability measurements performed on the plasma-polymerized coating allow to assert its hydrophobic feature, with WCA values of 107 ± 3°. This is a very significant

result that confirms the promising utilization of this coating to improve the perovskite film stability under moisture exposure [44,52–54].

The photographs of the pristine $MAPbI_3$ perovskite film and with the plasma deposited fluorocarbon coating (10, 30, 60, and 120 s of deposition time) are reported in Figure 3. The presence of the plasma-deposited coating can be observed by the naked eye as the deposition time increases. Indeed, a colour variation between the pristine sample (Figure 3a) and that obtained after 60 s (Figure 3d) and 120 s (Figure 3e) of the plasma deposition can be appreciated, because of the polymer thickness variation as a function of the deposition time. The thickness value of the pristine $MAPbI_3$ film corresponds to 440 ± 10 nm, while that of the perovskite after 60 s and 120 s of the plasma deposition is 488 ± 4 and 529 ± 9 nm, respectively (Table S1).



Figure 3. Photographs of: (**a**) pristine $MAPbI_3$ film; samples obtained by the plasma deposition of the fluorocarbon coating performed for (**b**) 10 s, (**c**) 30 s, (**d**) 60 s and (**e**) 120 s on the perovskite.

SEM images of the pristine perovskite film and of samples realized by depositing the fluorocarbon coatings on $MAPbI_3$ are displayed in Figures 4 and 5. They clearly show that the plasma processes do not negatively affect the perovskite morphology, rather they reduce the grain boundaries scattering. The plasma deposition of the fluorocarbon coating on the $MAPbI_3$ film creates a "fill effect" on the perovskite grains and allows us to observe a more uniform film for a longer deposition time. In this case, the morphology variation could be related to the coverage of the perovskite layer with the flat coating that, as discussed previously, is thicker for a longer deposition time. The flat character of the perfluorocarbon layer was observed by means of SEM analyses performed on the coating plasma-polymerized on glass substrates (Figure S1). This result was confirmed by AFM measurements carried out on a pristine $MAPbI_3$ film and on a sample obtained by the plasma deposition of the fluorocarbon coating of 60 s (Figure S2).

In Figure 5, the UV-vis absorption and the PL spectra of pristine and coated $MAPbI_3$ films are reported. The UV-vis spectra (Figure 5a) all exhibit the same trend with the absorption onset at approximately 780 nm, typical of the $MAPbI_3$ perovskite [26,41]. This absorption onset remains constant also after the plasma deposition of the perfluorocarbon coating, indicating that the plasma processes have no effect on the bulk perovskite material properties, but they affect just the surface [38]. This is a preliminary assessment of the compatibility of the proposed treatment with the referential $MAPbI_3$ perovskite. The spectra in Figure 5b show how the fluorocarbon layer strongly improves the intensity of the steady state PL. All threatened samples show a more intense PL emission than the pristine material, we also noticed variations across the series, the short treatment time of 10 s leads to the strongest PL and a monotonic reduction of this emission starts from this point for longer deposition times. Previous reports show how up to a few nanometres solution deposited layers would monotonically increase the PL of perovskite thin film due to surface defects passivation [55]. The surface defect reduction is confirmed by time resolved PL investigations, which show how the 10 s treated samples show a much longer decay in comparison to the untreated sample inset panel b Figure 5. This knowledge well falls with what we found for the 10 s deposited fluorocarbon layer. Noticeably for longer deposition times, we start depositing a reasonably thick layer and, considering 0.7 $nm \cdot s^{-1}$ as the determined plasma deposition rate, for 120 s we would have up to about 80 nm thick layers. These very thick layers would represent an important perturbation for the light excitation/emission path, differently impacting the light entrance/exit at

diverse energies [56]. This translates to a reduced light emission from $MAPbI_3$ when thick protective fluorocarbon layers are deposited on the top of it. Further investigation is planned to clarify the protecting layer thickness effect on the light management properties of perovskite films.

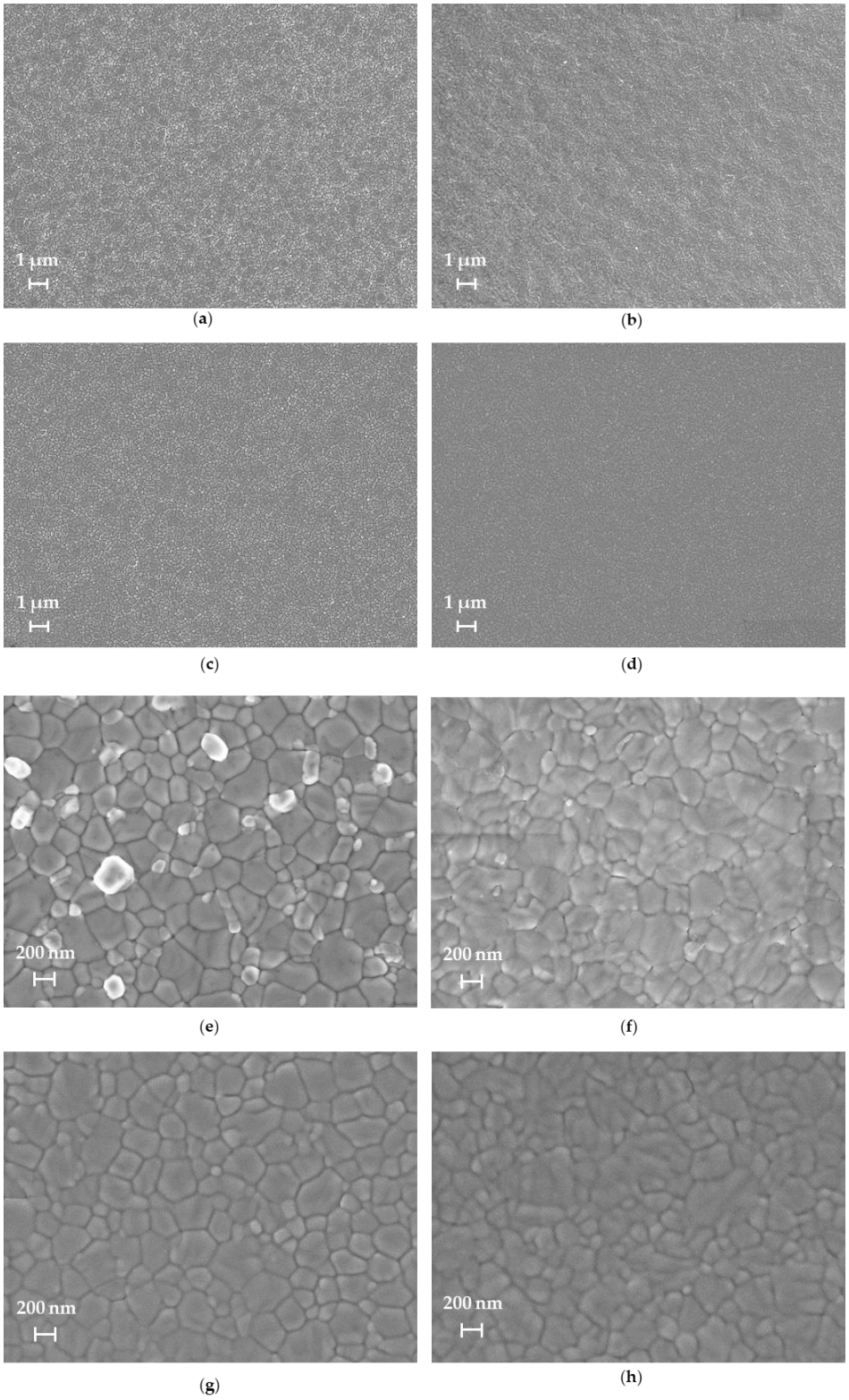


Figure 4. SEM images of: (**a**,**e**) pristine $MAPbI_3$ film; samples obtained by the plasma deposition of the fluorocarbon coating performed for (**b**,**f**) 10 s, (**c**,**g**) 30 s and (**d**,**h**) 60 s on the perovskite.

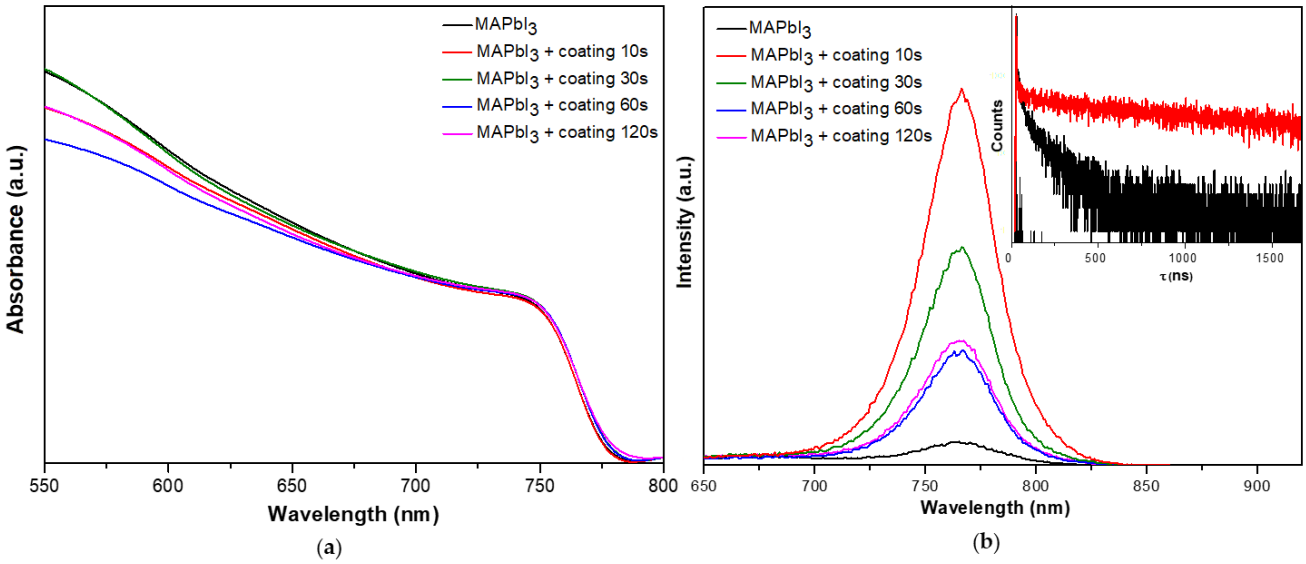


Figure 5. (**a**) UV-vis absorption spectra and (**b**) Steady-state PL spectra of pristine $MAPbI_3$ film and of samples obtained by the plasma deposition of the fluorocarbon coating performed for 10 s, 30 s, 60 s or 120 s on the perovskite. Inset panel (**b**) time resolved PL decay for $MAPI_3$ film and 10 s treated ones.

Photographs and UV-vis absorption spectra acquired to evaluate the stability in the air of pristine perovskite films and of samples realized by depositing the fluorocarbon coating on them are shown in Figures 6 and 7, respectively. The comparison between the collected results allows us to assert that the presence of the plasma-deposited coating increases the stability of $MAPbI_3$ films exposed to air (humidity range: 35–48%). In fact, the degradation of the pristine perovskite films takes place completely in just two weeks of air exposure, as demonstrated by the change in colour (Figure 6) as well as by the dramatic variation in the UV-vis spectrum with respect to the fresh sample (Figure 7a,b). These observations are both consistent with the breakdown of the $MAPbI_3$ structure and the subsequent presence of PbI_2 in the degraded layer [18,26–28]. On the contrary, samples obtained after the plasma deposition of the fluorocarbon coating on the perovskite carried out for 10 s show only a partial degradation after two weeks of exposure to air, preserving its absorption onset related to the perovskite optoelectronic properties, and exhibit a complete degradation after six weeks of storage in air (Figures 6 and 7c). Furthermore, samples obtained after the plasma deposition of the fluorocarbon coating on the perovskite carried out for 60 s do not show a complete degradation even after eight weeks of exposure to open air (Figure 6), continuing to present the absorption characteristics typical of $MAPbI_3$ perovskite films (Figure 7d) [26,41].

In Figure 8 photographs of pristine perovskite films and of samples obtained after the plasma deposition of the fluorocarbon coating, stored in a glass chamber at a humidity of 50% (temperature of 25 °C), are reported. The images show differences in terms of degradation times between the pristine $MAPbI_3$ and those on which the coating was deposited via plasma processes performed for 10 s and 60 s, as demonstrated by their change in colour [27,28]. Particularly, the degradation of the pristine perovskite film takes place just after 12 h of exposure to the humidity of 50%, while perovskite films with the plasma-deposited layer start to significantly degrade after 48 h of storage in the humid chamber. These preliminary results and those obtained for samples stored in open air are very significant and confirm the positive effect of the fluorocarbon coating on the $MAPbI_3$ stability. This aspect is very important for the subsequent possible use of the perovskite films (i.e., photovoltaic or photocatalytic technologies), opening new opportunities for the use of non-equilibrium plasma processes in the MHPs exploitation.

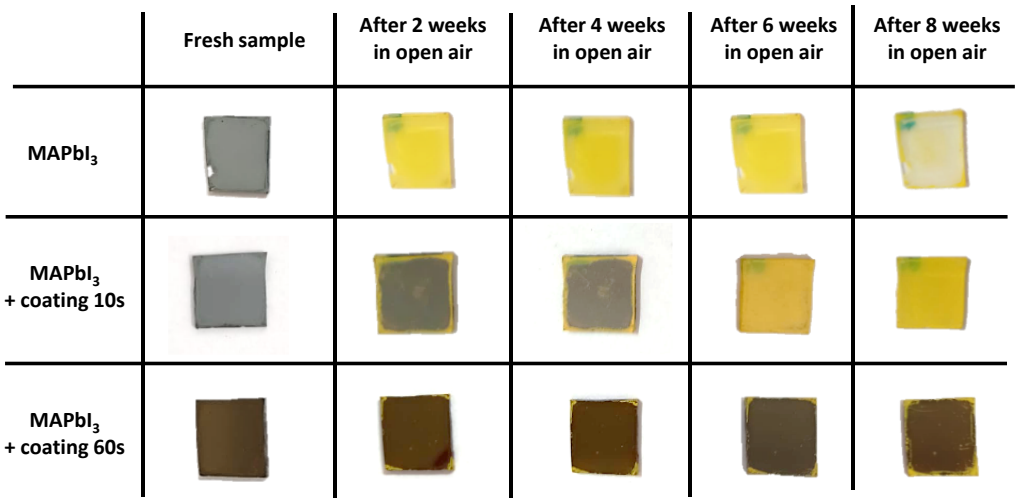


Figure 6. Photographs of pristine $MAPbI_3$ film and of samples obtained after the plasma deposition (10 and 60 s) of the fluorocarbon coating on the perovskite at different times of exposure to open air (0–8 weeks).

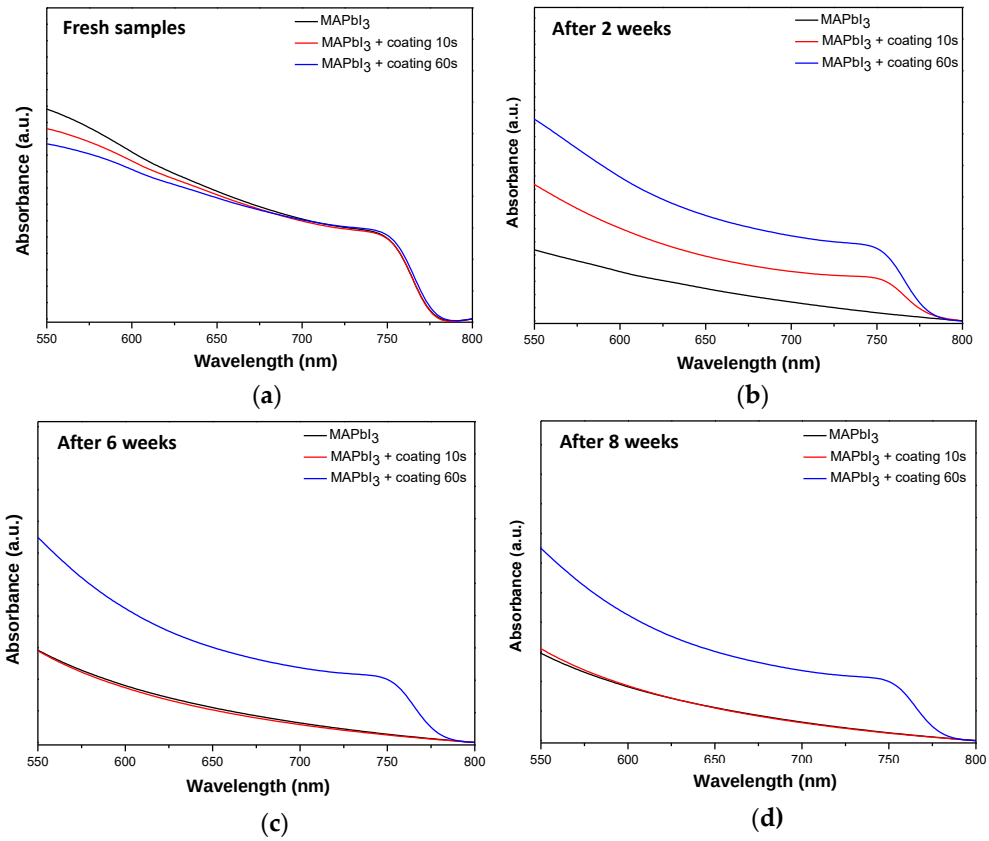


Figure 7. UV-vis absorption spectra of pristine $MAPbI_3$ film and of samples obtained after the plasma deposition (10 and 60 s) of the fluorocarbon coating on the perovskite after (**a**) 0 week (i.e., fresh), (**b**) 2 weeks, (**c**) 6 weeks and (**d**) 8 weeks of exposure to open air.

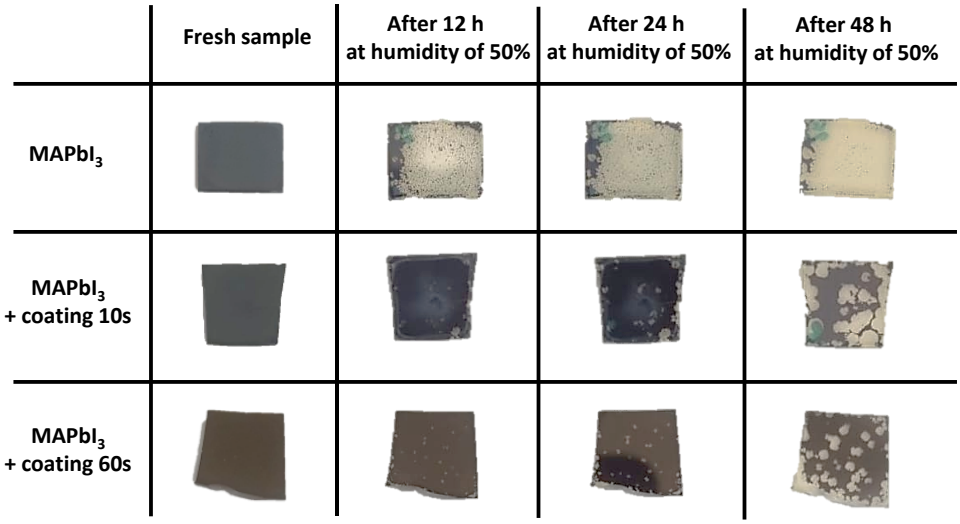


Figure 8. Photographs of pristine $MAPbI_3$ film and of samples obtained after the plasma deposition (10 and 60 s) of the fluorocarbon coating on the perovskite at different times of storage (0, 12, 24 and 48 h) in a sealed glass chamber at humidity of 50% and temperature of 25 °C.

4. Conclusions

In this work, we explored the effect of the plasma enhanced chemical vapour deposition of fluorocarbon coatings for $MAPbI_3$ film protection. Our aim was to investigate for the first time the application of plasma deposited coatings to challenging material such as MHP, to improve its resistance to humidity, and to study the effect on the MHP properties. We screened different deposition conditions to establish the best compromise between the preservation of the morphology, the enhancement of perovskite optical properties due to the surface defects passivation, and the improved resistance to moisture due to the hydrophobic character of the fluorinated polymer. The combined experimental analysis, SEM, absorption/emission spectroscopies, and stability tests monitoring the perovskite degradation, established that a plasma deposition process of 10 s, corresponding to a polymer thickness of about 7 nm, could be a good compromise, enhancing the photoluminescence intensity, that is considered a good indication of defects passivation, and improving the resistance to the film exposure both to ambient conditions and to a sealed chamber with 50% humidity value. This strategy can be extended to other MHP materials opening new opportunities in the use of plasmas for the modification of these materials and will be further tested in the fabrication of photovoltaic devices and/or photocatalytic technologies.

Supplementary Materials: The following supporting information can be downloaded at: https://www.mdpi.com/article/10.3390/en15134512/s1, Figure S1. SEM images of the fluorocarbon coating deposited in (a,b) 10 s and (c,d) 120 s on a glass substrate; Figure S2. AFM images of the (a,b) pristine $MAPbI_3$ film (RMS = 44.8 nm) and of (c,d) samples obtained by the plasma deposition of the fluorocarbon coating performed for 60 s on the perovskite (RMS = 14.9 nm); Table S1. Thickness values of pristine $MAPbI_3$ film and of samples obtained by the plasma deposition of the fluorocarbon coating performed for different time on the perovskite; Table S2. WCA values of fluorocarbon coatings deposited in different time.

Author Contributions: V.A. wrote the main body of the paper. A.M., S.C. and A.L. revised the paper. V.A., S.C., A.M., F.P. and F.F. performed the experiments. All authors have read and agreed to the published version of the manuscript.

Funding: This research was funded by the Puglia regional council (Grant name: Perseo, CUP: H95F20000890003).

Institutional Review Board Statement: Not applicable.

Informed Consent Statement: Not applicable.

Data Availability Statement: Not applicable.

Acknowledgments: Giuseppe D'Amato, Danilo Benedetti and Savino Cosmai are gratefully acknowledged for their practical and technical support.

Conflicts of Interest: The authors declare no conflict of interest.

References

1. d'Agostino, R.; Favia, P.; Fracassi, F. *Plasma Processing of Polymers*; NATO ASI Series; Kluwer Academic: Dordrecht, The Netherlands; Boston, MA, USA; London, UK, 1996.
2. Raitzer, Y.P. *Gas Discharge Physics*; Springer: Berlin, Germany, 1991.
3. Fridman, A.; Chirokov, A.; Gutsol, A. Non-thermal atmospheric pressure discharges. *J. Phys. D Appl. Phys.* **2005**, *38*, R1–R24. [CrossRef]
4. Kogelschatz, U. Dielectric-barrier discharges: Their history, discharge physics, and industrial applications. *Plasma Chem. Plasma Process.* **2003**, *23*, 1–46. [CrossRef]
5. d'Agostino, R. *Plasma Deposition, Treatment and Etching of Polymers*; Academic Press Inc.: San Diego, CA, USA, 1990.
6. Fanelli, F.; Fracassi, F. Atmospheric pressure non-equilibrium plasma jet technology: General features, specificities and applications in surface processing of materials. *Surf. Coat. Technol.* **2017**, *322*, 174–201. [CrossRef]
7. Armenise, V.; Gristina, R.; Favia, P.; Cosmai, S.; Fracassi, F.; Sardella, E. Plasma-Assisted Deposition of Magnesium-Containing Coatings on Porous Scaffolds for Bone Tissue Engineering. *Coatings* **2020**, *10*, 356. [CrossRef]
8. Trizio, I.; Intranuovo, F.; Gristina, R.; Dilecce, G.; Favia, P. He/O_2 Atmospheric Pressure Plasma Jet Treatments of PCL Scaffolds for Tissue Engineering and Regenerative Medicine. *Plasma Process. Polym.* **2015**, *12*, 1451–1458. [CrossRef]
9. Oliveira Zille, F.R.; Souto, A.P. Plasma treatment in textile industry. *Plasma Process. Polym.* **2015**, *12*, 98–131. [CrossRef]
10. Armenise, V.; Fanelli, F.; Milella, A.; D'Accolti, L.; Uricchio, A.; Fracassi, F. Atmospheric pressure plasma treatment of polyurethane foams with He–O2 fed dielectric barrier discharges. *Surfaces Interfaces* **2020**, *20*, 100600. [CrossRef]
11. Armenise, V.; Milella, A.; Fracassi, F.; Bosso, P.; Fanelli, F. Deposition of thin films containing carboxylic acid groups on polyurethane foams by atmospheric pressure non-equilibrium plasma jet. *Surf. Coat. Technol.* **2019**, *379*, 125017. [CrossRef]
12. Bosso, P.; Milella, A.; Barucca, G.; Mengucci, P.; Armenise, V.; Fanelli, F.; Giannuzzi, R.; Maiorano, V.; Fracassi, F. Plasma-assisted deposition of iron oxide thin films for photoelectrochemical water splitting. *Plasma Process. Polym.* **2020**, *18*, e2000121. [CrossRef]
13. Chen, F.; Song, J.; Liu, Z.; Liu, J.; Zheng, H.; Huang, S.; Sun, J.; Xu, W.; Liu, X. Atmospheric Pressure Plasma Functionalized Polymer Mesh: An Environment-friendly and Efficient Tool for Oil/Water Separation. *ACS Sustain. Chem. Eng.* **2016**, *4*, 6828–6837. [CrossRef]
14. A decade of perovskite photovoltaics. *Nat. Energy* **2019**, *4*, 1. [CrossRef]
15. Stranks, S.D.; Snaith, H.J. Metal-halide perovskites for photovoltaic and light-emitting devices. *Nat. Nanotechnol.* **2015**, *10*, 391–402. [CrossRef]
16. Huang, H.; Pradhan, B.; Hofkens, J.; Roeffaers, M.B.J.; Steele, J.A. Solar-Driven Metal Halide Perovskite Photocatalysis: Design, Stability, and Performance. *ACS Energy Lett.* **2020**, *5*, 1107–1123. [CrossRef]
17. Huynh, K.A.; Nguyen, D.L.T.; Nguyen, V.H.; Vo, D.V.N.; Trinh, Q.T.; Nguyen, T.P.; Kim, S.Y.; Le, Q.V. Halide perovskite photocatalysis: Progress and perspectives. *J. Chem. Technol. Biotechnol.* **2020**, *95*, 2579–2596. [CrossRef]
18. Armenise, V.; Colella, S.; Fracassi, F.; Listorti, A. Lead-Free Metal Halide Perovskites for Hydrogen Evolution from Aqueous Solutions. *Nanomaterials* **2021**, *11*, 433. [CrossRef]
19. Colella, S.; Mazzeo, M.; Rizzo, A.; Gigli, G.; Listorti, A. The Bright Side of Perovskites. *J. Phys. Chem. Lett.* **2016**, *7*, 4322–4334. [CrossRef]
20. Masi, S.; Aiello, F.; Listorti, A.; Balzano, F.; Altamura, D.; Giannini, C.; Caliandro, R.; Uccello-Barretta, G.; Rizzo, A.; Colella, S. Connecting the solution chemistry of PbI_2 and MAI: A cyclodextrin-based supramolecular approach to the formation of hybrid halide perovskites. *Chem. Sci.* **2018**, *9*, 3200–3208. [CrossRef]
21. Alberti, A.; Deretzis, I.; Mannino, G.; Smecca, E.; Giannazzo, F.; Listorti, A.; Colella, S.; Masi, S.; La Magna, A. Nitrogen Soaking Promotes Lattice Recovery in Polycrystalline Hybrid Perovskites. *Adv. Energy Mater.* **2019**, *9*, 1803450. [CrossRef]
22. Masi, S.; Sestu, N.; Valenzano, V.; Higashino, T.; Imahori, H.; Saba, M.; Bongiovanni, G.; Armenise, V.; Milella, A.; Gigli, G.; et al. Simple Processing Additive-Driven 20% Efficiency for Inverted Planar Heterojunction Perovskite Solar Cells. *ACS Appl. Mater. Interfaces* **2020**, *12*, 18431–18436. [CrossRef]
23. Giuri, A.; Rolston, N.; Colella, S.; Listorti, A.; Esposito Corcione, C.; Elmaraghi, H.; Lauciello, S.; Dauskardt, R.H.; Rizzo, A. Robust, High-Performing Maize–Perovskite-Based Solar Cells with Improved Stability. *ACS Appl. Energy Mater.* **2021**, *4*, 11194–11203. [CrossRef]
24. Rizzo, A.; Listorti, A.; Colella, S. Chemical insights into perovskite ink stability. *Chem* **2022**, *8*, 31–45. [CrossRef]
25. Bisconti, F.; Giuri, A.; Marra, G.; Savoini, A.; Fumo, P.; Marrazzo, R.; Zanardi, S.; Corso, G.; Po, R.; Biagini, P.; et al. Polymer-Assisted Single-Step Slot-Die Coating of Flexible Perovskite Solar Cells at Mild Temperature from Dimethyl Sulfoxide. *Chem. Plus Chem.* **2021**, *86*, 1442–1450. [CrossRef] [PubMed]

26. Bryant, D.; Aristidou, N.; Pont, S.; Sanchez-Molina, I.; Chotchunangatchaval, T.; Wheeler, S.; Durrant, J.R.; Haque, S.A. Light and oxygen induced degradation limits the operational stability of methylammonium lead triiodide perovskite solar cells. *Energy Environ. Sci.* **2016**, *9*, 1655–1660. [CrossRef]
27. Tolouenia, P.; Khassaf, H.; Amin, A.S.; Tobin, Z.M.; Alpay, S.P.; Suib, S.L. Moisture-Induced Structural Degradation in Methylammonium Lead Iodide Perovskite Thin Films. *ACS Appl. Energy Mater.* **2020**, *3*, 8240–8248. [CrossRef]
28. Hailegnaw, B.; Kirmayer, S.; Edri, E.; Hodes, G.; Cahen, D. Rain on Methylammonium Lead Iodide Based Perovskites: Possible Environmental Effects of Perovskite Solar Cells. *J. Phys. Chem. Lett.* **2015**, *6*, 1543–1547. [CrossRef] [PubMed]
29. Han, C.; Zhu, X.; Martin, J.S.; Lin, Y.; Spears, S.; Yan, Y. Recent Progress in Engineering Metal Halide Perovskites for Efficient Visible-Light-Driven Photocatalysis. *ChemSusChem* **2020**, *13*, 4005–4025. [CrossRef]
30. Giuri, A.; Masi, S.; Listorti, A.; Gigli, G.; Colella, S.; Corcione, C.E.; Rizzo, A. Polymeric rheology modifier allows single-step coating of perovskite ink for highly efficient and stable solar cells. *Nano Energy* **2018**, *54*, 400–408. [CrossRef]
31. Radicchi, E.; Ambrosio, F.; Mosconi, E.; Alasmari, A.A.; Alasmary, F.A.S.; De Angelis, F. Combined Computational and Experimental Investigation on the Nature of Hydrated Iodoplumbate Complexes: Insights into the Dual Role of Water in Perovskite Precursor Solutions. *J. Phys. Chem. B* **2020**, *124*, 11481–11490. [CrossRef]
32. Kaiser, W.; Ricciarelli, D.; Mosconi, E.; Alothman, A.A.; Ambrosio, F.; De Angelis, F. Stability of Tin- versus Lead-Halide Perovskites: Ab Initio Molecular Dynamics Simulations of Perovskite/Water Interfaces. *J. Phys. Chem. Lett.* **2022**, *13*, 2321–2329. [CrossRef]
33. Kim, H.-P.; Kim, M.; Kim, K.-B.; Khachatryan, H.; Jang, J. Properties of atmospheric-hydrogen-plasma-treated $CH_3NH_3PbI_3$ perovskite films. *Surf. Coat. Technol.* **2017**, *330*, 228–233. [CrossRef]
34. Xiao, X.; Bao, C.; Fang, Y.; Dai, J.; Ecker, B.R.; Wang, C.; Lin, Y.; Tang, S.; Liu, Y.; Deng, Y.; et al. Argon Plasma Treatment to Tune Perovskite Surface Composition for High Efficiency Solar Cells and Fast Photodetectors. *Adv. Mater.* **2018**, *30*, 1705176. [CrossRef]
35. Li, S.; Guo, T.; Li, Y.; Yun, S.; Xu, H.; Li, H.; Huang, A. Construction of nanostructured $CH_3NH_3PbI_3$ layer for high-performance perovskite solar cells by Ar plasma etching. *Mater. Res. Bull.* **2022**, *147*, 111666. [CrossRef]
36. Shekargoftar, M.; Jurmanová, J.; Homola, T. A Study on the Effect of Ambient Air Plasma Treatment on the Properties of Methylammonium Lead Halide Perovskite Films. *Metals* **2019**, *9*, 991. [CrossRef]
37. Zardetto, V.; Williams, B.L.; Perrotta, A.; Di Giacomo, F.; Verheijen, M.A.; Andriessen, R.; Kessels, W.M.M.; Creatore, M. Atomic layer deposition for perovskite solar cells: Research status, opportunities and challenges. *Sustain. Energy Fuels* **2017**, *1*, 30–55. [CrossRef]
38. Godding, J.S.; Ramadan, A.; Lin, Y.-H.; Schutt, K.; Snaith, H.J.; Wenger, B. Oxidative Passivation of Metal Halide Perovskites. *Joule* **2019**, *3*, 2716–2731. [CrossRef]
39. Chen, Z.-C.; Cheng, Y.; Lin, C.-C.; Li, C.-S.; Hsu, C.-C.; Chen, J.-Z.; Wu, C.-I.; Cheng, I.-C. In-situ atmospheric-pressure dielectric barrier discharge plasma treated $CH_3NH_3PbI_3$ for perovskite solar cells in regular architecture. *Appl. Surf. Sci.* **2018**, *473*, 468–475. [CrossRef]
40. Tsai, J.-H.; Cheng, I.-C.; Hsu, C.-C.; Chueh, C.-C.; Chen, J.-Z. Feasibility study of atmospheric-pressure dielectric barrier discharge treatment on $CH_3NH_3PbI_3$ films for inverted planar perovskite solar cells. *Electrochim. Acta* **2018**, *293*, 1–7. [CrossRef]
41. Shekargoftar, M.; Pospisil, J.; Dugáček, J.; Weiter, M.; Homola, T. Surface Property Tuning of Methylammonium Lead Iodide by Plasma for Use in Planar Perovskite Solar Cells. *ACS Omega* **2020**, *5*, 18384–18390. [CrossRef]
42. Kumar, V.; Pulpytel, J.; Arefi-Khonsari, F. Fluorocarbon Coatings Via Plasma Enhanced Chemical Vapor Deposition of 1H,1H,2H,2H-perfluorodecyl Acrylate-1, Spectroscopic Characterization by FT-IR and XPS. *Plasma Process. Polym.* **2010**, *7*, 939–950. [CrossRef]
43. d'Agostino, R.; Favia, P.; Ikegami, H.; Kawai, Y.; Sato, N.; Arefi-Khonsari, F. *Advanced Plasma Technology*; Wiley-VCH: Weinheim, Germany, 2007.
44. Wu, C.; Wang, K.; Feng, X.; Jiang, Y.; Yang, D.; Hou, Y.; Yan, Y.; Sanghadasa, M.; Priya, S. Ultrahigh Durability Perovskite Solar Cells. *Nano Lett.* **2019**, *19*, 1251–1259. [CrossRef]
45. Favia, P.; Cicala, G.; Milella, A.; Palumbo, F.; Rossini, P.; D'Agostino, R. Deposition of super-hydrophobic fluorocarbon coatings in modulated RF glow discharges. *Surf. Coat. Technol.* **2003**, *169*, 609–612. [CrossRef]
46. Intranuovo, F.; Sardella, E.; Rossini, P.; d'Agostino, R.; Favia, P. PECVD of Fluorocarbon Coatings from HexafluoropropyleneOxide: Glow vs. Afterglow. *Chem. Vap. Depos.* **2009**, *15*, 95–100. [CrossRef]
47. Limb, S.J.; Gleason, K.K. Flexible fluorocarbon wire coatings by pulsed plasma enhanced chemical vapor deposition. *J. Vac. Sci. Technol. A* **1997**, *15*, 1814–1818. [CrossRef]
48. Lapenna, A.; Fanelli, F.; Fracassi, F.; Armenise, V.; Angarano, V.; Palazzo, G.; Mallardi, A. Direct Exposure of Dry Enzymes to Atmospheric Pressure Non-Equilibrium Plasmas: The Case of Tyrosinase. *Materials* **2020**, *13*, 2181. [CrossRef]
49. Bosso, P.; Milella, A.; Armenise, V.; Fanelli, F.; Fracassi, F. Hybrid perfluorocarbon/carboxylic acid thin films via plasma deposition of hexafluoropropene and acrylic acid mixtures. *Vacuum* **2021**, *184*, 109933. [CrossRef]
50. Romani, L.; Speltini, A.; Nazareno Dibenedetto, C.; Listorti, A.; Ambrosio, F.; Mosconi, E.; Simbula, A.; Saba, M.; Profumo, A.; Quadrelli, P.; et al. Experimental Strategy and Mechanistic View to Boost the Photocatalytic Ac-tivity of Cs3Bi2Br9 Lead-Free Perovskite Derivative by g-C3N4 Composite Engineering. *Adv. Funct. Mater.* **2021**, *31*, 2104428. [CrossRef]
51. Greczynski, G.; Hultman, L. Compromising Science by Ignorant Instrument Calibration—Need to Revisit Half a Century of Published XPS Data. *Angew. Chem.* **2020**, *59*, 5002–5006. [CrossRef]

52. Idígoras, J.; Aparicio, F.J.; Contreras-Bernal, L.; Ramos-Terrón, S.; Alcaire, M.; Sánchez-Valencia, J.R.; Borras, A.; Barranco, A.; Anta, J.A. Enhancing Moisture and Water Resistance in Perovskite Solar Cells by Encapsulation with Ultrathin Plasma Polymers. *ACS Appl. Mater. Interfaces* **2018**, *10*, 11587–11594. [CrossRef]
53. Kim, M.; Kang, T.-W.; Kim, S.H.; Jung, E.H.; Park, H.; Seo, J.; Lee, S.-J. Antireflective, self-cleaning and protective film by continuous sputtering of a plasma polymer on inorganic multilayer for perovskite solar cells application. *Sol. Energy Mater. Sol. Cells* **2018**, *191*, 55–61. [CrossRef]
54. Kim, J.; Lee, G.; Lee, K.; Yu, H.; Lee, J.W.; Yoon, C.M.; Kim, S.G.; Kim, S.K.; Jang, J. Fluorine plasma treatment on car-bon-based perovskite solar cells for rapid moisture protection layer formation and performance enhancement. *Chem. Commun.* **2020**, *56*, 535–538. [CrossRef]
55. Yang, F.; Lim, H.E.; Wang, F.; Ozaki, M.; Shimazaki, A.; Liu, J.; Mohamed, N.B.; Shinokita, K.; Miyauchi, Y.; Wakamiya, A.; et al. Roles of Polymer Layer in Enhanced Photovoltaic Performance of Perovskite Solar Cells via Interface Engineering. *Adv. Mater. Interfaces* **2018**, *5*, 1701256–1701265. [CrossRef]
56. Tooghi, A.; Fathi, D.; Eskandari, M. Numerical study of a highly efficient light trapping nanostructure of perovskite solar cell on a textured silicon substrate. *Sci. Rep.* **2020**, *10*, 18699–18712. [CrossRef] [PubMed]